

## Corrosion study of ferrites prepared by hydrothermal method

S.U. Rather

Department of Chemical and Materials Engineering, King Abdulaziz University,  
P.O. Box 80204, Jeddah 21589, Saudi Arabia

Received March 29, 2016; Revised August 13, 2016

Zinc and nickel ferrite have been synthesized from metal nitrates using a hydrothermal method to study the structural, thermal, and corrosion properties. The XRD pattern of both zinc and nickel ferrite confirm face centered cubic (FCC) spinel structure with a very small impurity phase of hematite ( $\alpha$ -Fe<sub>2</sub>O<sub>3</sub>). TGA and DSC shows two major weight losses, exothermic and endothermic, corresponding to moisture removal and decomposition of oxides to zinc/nickel ferrite. Sharp Auger electron peaks are visible throughout XPS spectrum of both ferrites. The corrosion protection of zinc ferrite is because of the unavailability of the metal for the redox pair reaction while cobalt ferrite corrosion protection is because of the passivation layer formed over time.

**Keywords:** Hydrothermal method, Ferrites, Potentiostat, Corrosion, Thermal decomposition, Working electrode

### INTRODUCTION

Spinel ferrite MFe<sub>2</sub>O<sub>4</sub>, where M indicates Ni, Zn, Co, Mn, etc. is a close packed structure with two different crystallographic sites, namely tetrahedral and octahedral. These sites are also referred to as A and B-sites, respectively. Spinel structure contains two cation sites for metal cation occupancy. There are 8 A-sites in which the metal cations are tetrahedrally coordinated with oxygen atoms and 16 B-sites, which are octahedrally coordinated. Three kinds of spinel ferrites are formed by the occupancy of A and B-sites with M<sup>2+</sup> and Fe<sup>3+</sup> cations. Normal spinel ferrite is when A-sites are occupied by M<sup>2+</sup> cations and the B-sites are occupied by Fe<sup>3+</sup> cations. Inverse spinel ferrite is when A-sites are completely occupied by Fe<sup>3+</sup> cations and B-sites are randomly occupied by M<sup>2+</sup> and Fe<sup>3+</sup> cations. In mixed spinel ferrite, both A and B-sites are occupied by M<sup>2+</sup> and Fe<sup>3+</sup> cations. Normal, inverse, and mixed spinel ferrite are shown in table 1.

**Table 1.** Normal, inverse and mixed spinel ferrite.

Site A	Site B	Ferrite Type
M <sup>2+</sup>	Fe <sup>3+</sup>	Normal spinel ferrite
Fe <sup>3+</sup>	M <sup>2+</sup>	Inverse spinel ferrite
M <sup>2+</sup> or Fe <sup>3+</sup>	M <sup>2+</sup> or Fe <sup>3+</sup>	Mixed spinel ferrite

Conventional size controlled co-precipitation [1], ultrasonic wave-assisted ball milling technology [2], co-precipitation [3], non-aqueous synthesis method [4], thermal treatment method [5-8], hydrothermal process [9], and polymerized complex method [10] were used to synthesize ferrite nanoparticles. Ferrites are nowadays quite often used as inductive

components in various electronic circuits. High frequency applications such as telecommunication and radar systems make ferrites the most essential part of advanced technology. Furthermore, ferrites are also used in computers, TV, video systems, small and medium power related instruments. Other important application of ferrites is: electromagnetic interference (EMI) suppression related to notebooks, cameras, digital computers, scanners, etc. and biosciences related to magnetic materials present in the nanoparticles, specifically magnetite (Fe<sub>2</sub>O<sub>3</sub>), in various forms of living organisms [11]. Corrosion protection by coating of ferrites on steel alloy samples is performed to avoid surface damage in hostile environmental conditions. Furthermore, it was proved that doping of ferrites with Nd-Co increases the corrosion protection and resistance against aggressive environment as compared to pristine ferrites [12]. Morphology and chemical composition of ferrites are very crucial to improve their anticorrosion properties [13]. Keeping in mind above-mentioned applications, study of corrosion properties of ferrites such as zinc ferrites, cobalt ferrites, nickel ferrites, etc. may help to improve applications in a more advanced manner in near future.

In this paper, synthesis, characterization, and corrosion properties of zinc and cobalt ferrites are reported. Main aim of this report is to study the corrosion properties of ferrites at different time intervals.

### EXPERIMENTAL

#### Materials and Preparation

Iron nitrate (Fe(NO<sub>3</sub>)<sub>3</sub> · 9H<sub>2</sub>O), zinc nitrate (Zn(NO<sub>3</sub>)<sub>2</sub> · 6H<sub>2</sub>O), and cobalt nitrate

\* To whom all correspondence should be sent:  
E-mail: rathersami@kau.edu.sa, rathersami@gmail.com

( $\text{Co}(\text{NO}_3)_3 \cdot 6\text{H}_2\text{O}$ ), were purchased from Acros Organics with a purity exceeding 99%. Poly(vinyl pyrrolidone) (PVP) (MW = 30,000) was purchased from Sigma Aldrich and all the above chemicals were used without further purification. For the preparation of zinc and cobalt ferrites, an aqueous solution of PVP was prepared by dissolving 3 g of polymer in 100 mL of distilled water at 363 K. 0.2 mmol iron nitrate and 0.1 mmol zinc nitrate/cobalt nitrate were mixed into the above polymer solution and constantly stirred for 2 h using a magnetic stirrer. A litmus paper was used to determine the pH of the solution, which ranged from 4 to 5. The mixed solution was heated at 80°C for 24 h to evaporate moisture. The dried, orange, solid zinc/cobalt ferrite that remained was crushed and grounded in a mortar to form fine powder. The calcination of the powders was conducted at 600°C for 3 h for the decomposition of organic compounds and the crystallization of the nanocrystals.

### Characterization

The structure of  $\text{ZnFe}_2\text{O}_4$  and  $\text{CoFe}_2\text{O}_4$  was characterized by XRD technique using an Inel X-Ray diffractometer model EQUINOX 1000 with CuK $\alpha$  radiation ( $k = 0.15406$  nm) to generate diffraction patterns from powder crystalline samples at ambient temperature in the  $2\theta$  range of 15 to 70°. Thermal decomposition and examination of the absorptive surfaces were conducted at 950°C using thermogravimetric analysis (TGA) and differential scanning calorimetric analysis (DSC) on a model STA 449 F3 Jupiter. XPS was performed using XPS SPEC GmbH, Germany.

### Measurement of Corrosion Properties

A three-electrode system is used to determine the Tafel curves for the ferrite powder in a 3.5% NaCl electrolyte solution. The working electrode is a compact ferrite powder in contact with a copper rod. Paraffin (C14) was used as a binder. The electrode is polarized to  $\pm 200$  mV with respect to the open circuit potential. The  $I_r$  resistance is measured by zero run without the sample and is adjusted. The Tafel curves are then used to determine the corrosion rates. The potentiostat used to polarize the ferrite electrode is provided by AUTOLAB. The NOVA software is used to analyze the results.

## RESULTS AND DISCUSSION

X-ray diffraction (XRD) was used to identify the structure of the zinc/cobalt ferrite samples. The patterns of zinc/cobalt ferrite as prepared and

calcined at 600°C are presented in Figs. 1 and 2. Peaks in the as prepared samples are not visible, but as calcination temperature increases to 600°C, sharp intense peaks appear. Both zinc and cobalt ferrite XRD patterns are characterized by several intense peaks between diffraction angle of 15 and 70°. The pattern shown in Fig. 1 is a form of cubic structure which is interpreted as cubic spinel zinc ferrite indexed by the peaks of (111), (220), (311), (222), (400), (331), (422), (511), and (440). Fig. 2 shows XRD pattern of as prepared and calcined cobalt ferrite samples. The peaks can be indexed to noticeable reflection from (111), (220), (311), (222), (400), (331), (422), (511), and (440) planes of cobalt ferrite. Both zinc and cobalt ferrite samples show very small impurity phase of  $\alpha\text{-Fe}_2\text{O}_3$  (H) and this impurity occurs naturally as hematite [14-16].

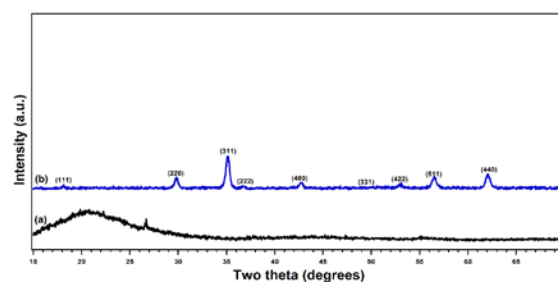


**Fig. 1.** X-ray diffraction (XRD) profile of zinc ferrite ( $\text{ZnFe}_2\text{O}_4$ ) synthesized by hydrothermal method.

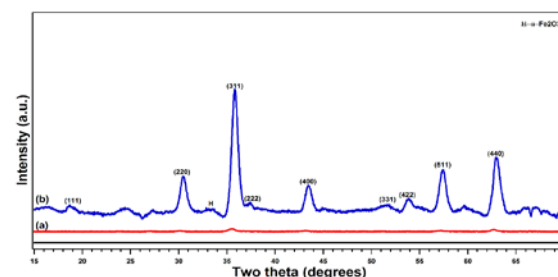


**Fig. 2.** X-ray diffraction (XRD) profile of cobalt ferrite ( $\text{CoFe}_2\text{O}_4$ ) prepared by hydrothermal method.

Thermal decomposition of as prepared zinc/cobalt ferrite samples was studied by TGA and DSC, presented in Figs. 3 and 4, respectively. Two major weight loss curves for zinc ferrite, from 75 to 125°C are due to evaporation of moisture. From 400 to 500°C weight loss is due to decomposition of elemental oxides, zinc oxide, and hematite ( $\text{Fe}_2\text{O}_3$ ) to the crystalline zinc ferrite. The extended curve after the last peak ( $>600^\circ\text{C}$ ) indicates sample stability and formation of crystalline zinc ferrite, as confirmed also by XRD. The corresponding DSC curve shows two major peaks, at 93°C, an endothermic peak indicates moisture removal and at 472°C, an exothermic peak confirms decomposition [17, 18]. Two major weight losses of cobalt ferrite were also observed, the first around

100°C indicates moisture removal and the second at 400-500°C, confirms decomposition of sample and formation of crystalline cobalt ferrite. The extended curve after the last peak (>600°C) indicates sample stability and formation of crystalline cobalt ferrite, as confirmed by XRD, following the same trend as zinc ferrite. DSC curve also shows two major peaks, an endothermic peak indicates moisture removal and an exothermic peak at 473°C confirms decomposition [19, 20].

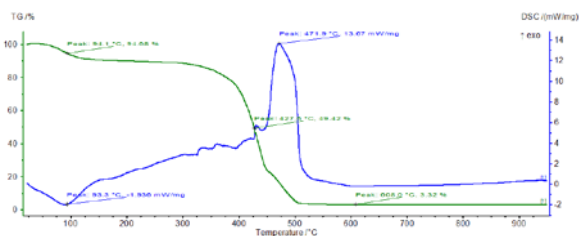


**Fig. 3.** Thermogravimetric analysis (TGA) and differential scanning calorimetry (DSC) data of zinc ferrite performed in an oxygen atmosphere. The heating ramp used is 10°C/min.

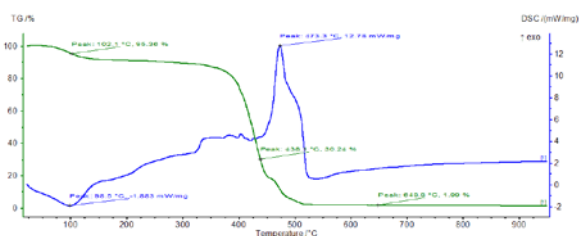


**Fig. 4.** Thermogravimetric analysis (TGA) and differential scanning calorimetry (DSC) data of cobalt ferrite performed in an oxygen atmosphere. The heating ramp used is 10°C/min.

XPS results of zinc and cobalt ferrites are presented in Figs. 5 and 6, where binding energy (BE) ranges from 0 to 1100 eV. Sharp Auger

electron peaks are visible throughout the XPS spectrum of zinc ferrite/cobalt ferrite. Core levels of Zn 2P, Co 2P, and Fe 2P are also visible. The presence of very low peaks of absorbed carbon on the spectra is due to PVP involved during the synthesis process [21].

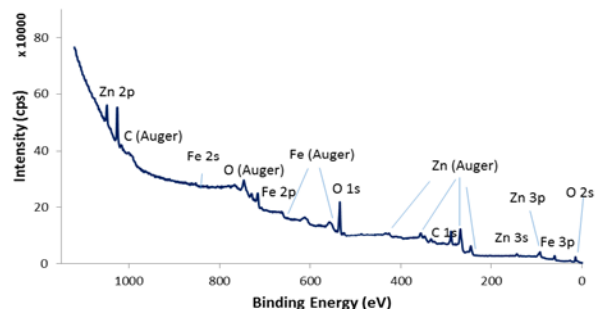


**Fig. 5.** Wide scan survey X-ray photoelectron spectra (XPS) of zinc ferrite ( $ZnFe_2O_4$ ).

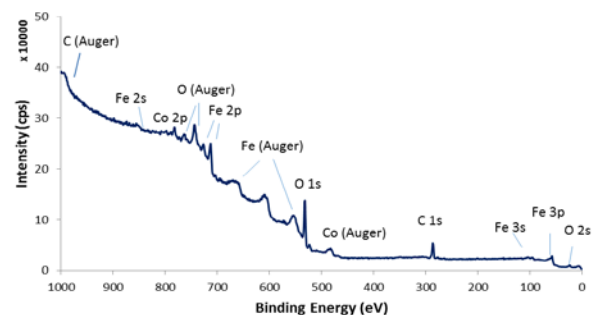


**Fig. 6.** Wide scan survey X-ray photoelectron spectra (XPS) of cobalt ferrite ( $CoFe_2O_4$ ).

Full details of both zinc and cobalt ferrite are presented in Tables 2 and 3.

**Table 2.** Quantitative analysis of XPS data of  $ZnFe_2O_4$

Sample Name	Name	Position	FWHM	Area / (T*MFP)	% At. Conc.	Mass	% Mass Conc.
Zn-Ferrite	Fe (Fe 2p <sub>3/2</sub> )	710.79	4.211	26355.1	11.79	55.8458	23.501
	O (O 1s)	529.99	3.609	44341.2	73.39	15.9994	41.911
	Zn (Zn 2p <sub>3/2</sub> )	1022.39	2.356	56527.1	14.82	65.3873	34.588
					100		100

**Table 3.** Quantitative analysis of XPS data of  $CoFe_2O_4$

Sample Name	Name	Position	FWHM	Area / (T*MFP)	% At. Conc.	Mass	% Mass Conc.
Co-Ferrite	Co (Co 2p)	780.04	4.533	34700.2	10.069	58.9332	21.779
	Fe (Fe 2p <sub>3/2</sub> )	710.34	3.844	32179.7	17.378	55.8458	35.618
	O (O 1s)	529.74	2.845	36520.7	72.553	15.9994	42.603
					100		100

The TAFEL curves for the zinc ferrite in saline solution are shown in Fig. 7. Zinc ferrite corrosion rates do not increase with time, essentially having constant anodic and cathodic surface reactions. This indicates that there is no change in the surface composition of zinc ferrite over time. Zinc ferrites anticorrosion pigments are embedded in various matrices of the paints/epoxy resins to enhance the anti-corrosion properties (22, 23). As the corrosion potential  $E_{cp}$  remains constant over the entire testing time period, therefore cathodic and anodic reactions and not the solid sample of the working electrode are the representation of the solution species (oxygen and water redox couple reactions). Thus, zinc ferrite does not show any metal dissolution into the solution. This is not true for the zinc nitrate and iron nitrate solid particles sintered below 600°C. Cobalt ferrite Tafel curves are shown in Fig. 8. Corrosion rate is almost constant over the entire testing period. However, the corrosion potential decreases over time. This indicates that there is some change on the surface of the cobalt ferrite that provides more resistance to polarization over the surface of the specimen. Cobalt is known to produce a passive layer if alloyed with steel under aggressive environment (24).

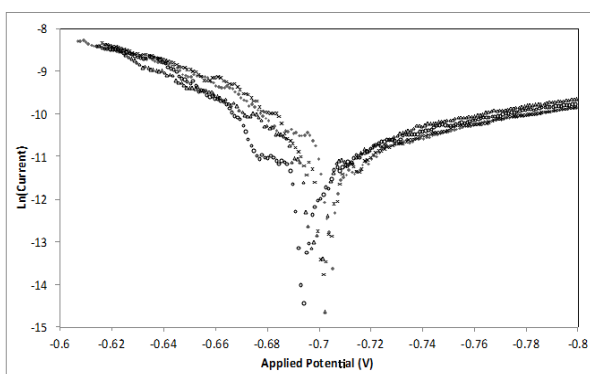


**Fig. 7.** Tafel curves of zinc ferrites over time, ( $\Delta$  - 3 min), ( $\circ$  - 30 min), ( $\times$  - 60 min), and ( $+$  - 120 min).

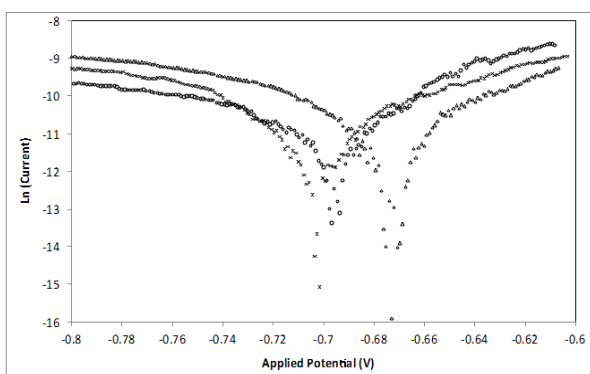


**Fig. 8.** Tafel curves of cobalt ferrite over time, ( $\Delta$  - 3 min), ( $\circ$  - 60 min), and ( $\times$  - 120 min).

## CONCLUSIONS

The results of this investigation indicate that thermal treatment method can be used for synthesis of  $ZnFe_2O_4$  and  $CoFe_2O_4$  nanoparticles using poly(vinyl pyrrolidone) as a capping agent to stabilize the particles and prevent them from agglomerating. XRD patterns indicate the presence of face centered cubic spinel structure with natural impurities. TGA curves shows two major peaks related to the weight losses due to water evaporation and decomposition to crystalline phase. XPS results show the percentages of elements present on the surface of the metal ferrites. The corrosion protection of zinc ferrite is because of the unavailability of the metals for the redox pair reaction. While cobalt ferrite corrosion protection is because of the passivation layer formed over time.

**Acknowledgements:** This research was funded by the Deanship of Scientific Research (DSR), King Abdulaziz University, Jeddah under grant No. D1435-974-135. The author, therefore, acknowledges with thanks DSR technical and financial support.

## REFERENCES

1. Y. Mattei, O. Pérez, O. Uwakweh, *J. Magn. Magn. Mater.*, **341**, 17 (2013).
2. D. Chenn, L. Li, J. Wang, *Ceram. Int.*, **39**, 4669 (2013).
3. M. El-Okr, M. Salem, M. Salem, M. Salim, *J. Magn. Magn. Mater.*, **323**, 920 (2009).
4. L. Ajroudi, S. Villain, V. Madigou, *J. Cryst. Growth*, **312**, 2465 (2010).
5. M.G. Naseri, E. B. Saion, H.A. Ahangar, A.H. Shaari, M. Hashim, *J. Nanomater.*, **1**, 1 (2010).
6. M.G. Naseri, E.B. Saion, H. A. Ahangar, A.H. Shaari, M. Hashim, *J. Powder Technol.*, **212**, 80 (2011).
7. M.G. Naseri, E.B. Saion, M. Hashim, A.H. Shaari, H.A. Ahangar, *J. Solid State Commun.*, **151**, 1031 (2011).
8. M. Stoia, P. Barvinschi, L. Tudoran, *J. Therm. Anal. Calorim.*, **108**, 1033 (2012).
9. M. Su, C. Hea, V. Sharma, *J. Hazard. Mater.*, **211**, 95 (2012).
10. S.M. Montemayor, L.A. Garcí'a-Cerda, J.R. Torres-Lubia'n, *Mater. Lett.*, **59**, 1056 (2005).
11. R. Valenzuela, *Phys. Res. Int.*, **2012**, 1 (2012).
12. C.A. Herme, G.P. Cicileo, P.G. Bercoff, S.E. Jacobo, *Pro. Mater. Sci.*, **9**, 150 (2015).
13. A. Kalendová, P. Rysánek, K. Nechvílová, *Prog. Org. Coat.*, **86**, 147 (2015).
14. J. Vidales, A. Lopez-Delgado, E. Vila, *J. Alloys Compd.*, **287**, 276 (1999).
15. M. Naseri, E. Saion, H. Ahangar, *J. Nanomater.*, **2010**, 1(2010).

16. Y. Qu, H. Yang, N. Yang, *J. Mater. Lett.*, **60**, 3548 (2006).
17. P. Aghav, V. Dhage, M. Mane, *J. Phys. B*, **406**, 4350 (2011).
18. P. Laokul, V. Amornkitbamrung, S. Seraphin, *J. Curr. Appl. Phys.*, **11**, 101 (2011).
19. B. Randhawa, M. Gupta, M. Kaur, *J. Ceram. Int.*, **35**, 3521 (2009).
20. S. Rana, J. Philip, B. Raj, *J. Mater. Chem. Phys.*, **124**, 264 (2010).
21. G. Fan, Z. Gu, L. Yang, F. Li, *J. Chem. Eng.*, **155**, 534 (2009).
22. Y.M.A. Ayana, S.M. El-Sawy, S.H. Salah, *Anticorr. Meth. Mater.* **44**, 381 (1997).
23. A.M. Musa, N.N. Shawal, H.U. dadum, M. Jibril, G. Abdurrahman, M.Z. Husna, *Appl. Mech. Mater.*, **695**, 110 (2015).
24. K.H. Kim, S.H. Lee, N.D. Nam, J.G. Kim, *Corr. Sci.*, **53**, 3576 (2011).

## ИЗСЛЕДВАНЕ НА КОРОЗИЯТА НА ФЕРИТИ, ПРИГОТВЕНИ ПО ХИДРОТЕРМАЛЕН МЕТОД

С.У. Ратхер

*Департамент по химично инженерство и материалознание, Университет „Крал Абдулазиз“, Джеда, Саудитска Арабия*

Постъпила на 29 март, 2016 г.; приета на 13 август, 2016 г.

(Резюме)

Цинковите и никеловите ферити се синтезират от метални нитрати по хидротермален метод, за да се изследват структурните, термичните и корозионните им свойства. Рентгено-структурните характеристики на двата ферита потвърждават челно-центрираната кубична (FCC) шпинелова структура с малки онечистван от хематит ( $\alpha$ -Fe<sub>2</sub>O<sub>3</sub>). Термогравиметричният анализ и диференциално-сканиращата калориметрия показват две главни загуби на тегло (екзотермична и ендотермична), съответстващи на отстраняване на влага и разлагане на оксидите във феритите. Остри и Оже-електронни пикове се забелязват в рентгено-структурните спектри на двата ферита. Защитата от корозия на цинковия ферит се дължи на недостъпността на метала към редокс-реакции, докато корозионната защита при кобалтовия ферит се дължи на пасивиращия слой, формиран с времето.